Chaos

Swing equation in power systems: Approximate analytical solution and bifurcation curve estimate

Cite as: Chaos **30**, 013110 (2020); https://doi.org/10.1063/1.5115527
Submitted: 19 June 2019 . Accepted: 17 December 2019 . Published Online: 07 January 2020

Qi Qiu, Rui Ma, Jurgen Kurths, and Meng Zhan

COLLECTIONS

Paper published as part of the special topic on Dynamics of Modern Power Grids
Note: This paper is part of the Focus Issue on the Dynamics of Modern Power Grids.

Chaos ARTICLE scitation.org/journal/cha

Swing equation in power systems: Approximate analytical solution and bifurcation curve estimate

Cite as: Chaos 30, 013110 (2020); doi: 10.1063/1.5115527
Submitted: 19 June 2019 · Accepted: 17 December 2019 ·
Published Online: 7 January 2020

Qi Qiu,[1] Rui Ma,[1] Jurgen Kurths,[2,3,4] and Meng Zhan[1,a)]

AFFILIATIONS

[1] State Key Laboratory of Advanced Electromagnetic Engineering and Technology, School of Electrical and Electronic Engineering, Huazhong University of Science and Technology, Wuhan 430074, China
[2] Potsdam Institute for Climate Impact Research, Telegraphenberg, Potsdam D-14415, Germany
[3] Institute of Physics, Humboldt University Berlin, Berlin D-12489, Germany
[4] Saratov State University, Saratov 4410012, Russia

Note: This paper is part of the Focus Issue on the Dynamics of Modern Power Grids.
[a)] **Author to whom correspondence should be addressed:** zhanmeng@hust.edu.cn

ABSTRACT

The swing equation plays a central role in the model and analysis of power system dynamics, including small-signal stability and transient stability. As it has the same form as that in a variety of different disciplines, such as the forced pendulum in mechanics, the classical mechanistic description of superconducting Josephson junctions in physics, and the classical second-order phase-locking loop in electronics, it has aroused general interest in science and engineering. In this paper, its approximate solution of the limit cycle is obtained by means of the incremental harmonic balance (IHB) method. It is found that the trouble of a more distorted limit cycle when the parameters are closer to the homoclinic bifurcation curve can be easily solved by incorporating higher order harmonics in the IHB method. In this way, we can predict the homoclinic bifurcation curve perfectly. In addition, the method is extended to study a generalized swing equation including excitation voltage dynamics.

Due to the increasing pressure of environmental protection and energy resource, our modern societies are vigorously supporting the development of various renewable energies, in particular, wind power and photovoltaics.[1] Large-scale distributed power sources interfaced with converters have been integrated into power grids in recent years. The power electric system is becoming gradually more power-electronics-based, relying on controllers in converters, and meanwhile, its dynamics behavior is becoming much more complicated compared to that of traditional power systems.[1–6] In traditional power systems, based on Newton's second equation of motion, the swing equation characterizes the rotor's motion of a synchronous generator under the imbalanced torque and plays a key contribution to our understanding of power system electromechanical dynamics.[7–11] Thus, it is not surprising to see that, even in studying the power-electronics-based power system, researchers are trying to use a similar equation resembling the dynamics of a synchronous generator to understand and/or control its dynamical behavior. For example, virtual synchronous generators[12,13] and power-synchronization control methods[14] have been proposed to modify the control algorithms of converters and resemble the dynamic behavior of a synchronous machine. A novel model of the amplitude-phase motion equation has also been advocated to extend the swing equation by including an additional equation for the voltage amplitude.[3–5] Thus, the classical swing equation is important for our understanding of power system dynamics. However, to the best knowledge of the authors, an approximate analytical solution for periodic motion (limit cycle) and the set of parameters corresponding to the homoclinic separatrix are still unavailable. The objective of this work just aims to solve these unsolved problems by using an incremental harmonic balance method.

I. INTRODUCTION

In traditional power systems, the electromechanical dynamics of a synchronous generator is dominated by its rotor motion, which is represented by a well-known second-order differential equation, the swing equation in the simplest form.[15–21] It plays a dominant role in many basic problems in power systems, such as rotor-angle stability in a single-machine-infinite-bus system and also in coupled multiple machine systems, low-frequency oscillation, and subsynchronous oscillation. This equation is highly nonlinear. In many situations, such as small-signal stability analysis and design of linear controllers, the swing equation is linearized and thus only the stability of the so-called working point (i.e., fixed point) is concerned. However, in the transient stability analysis, we have to deal with its nonlinearity, and thus various dynamical behaviors including fixed points and limit cycle are of interest. In particular, the transient stability is determined by the system state and the basin of attraction of the postfault working point. This is essentially a global stability problem in the language of nonlinear dynamics, and both the fixed point and the coexisting limit cycle are of importance. Therefore, fully grasping the complicated dynamics in the swing equation (or the so-called second-order Kuramoto equation) and even in the coupled swing equations is significant. It is only natural to see that these studies have become a hot topic in nonlinear dynamics and complex systems science recently.[22–28]

In addition, the significance of a nonlinear study of the swing equation is also supported by the fact that it is, in mathematics, exactly the same as the dynamic equations in many other systems, such as forced pendulum in mechanics, the classical mechanistic description of superconducting Josephson junctions in physics, and the classical second-order phase-locking loop in electronics.[29,30] A similar model system is the motion of a mechanical particle in a tilted washboard potential in stochastic dynamical systems.[31–33] This mechanical analog has been analyzed in detail in statistical physics; see a recent paper and references therein.[34]

The basic physical picture of the swing equation has been well established and recognized, including three distinct dynamic regimes: stable fixed point, stable limit cycle, and their coexistence for different initial conditions, depending on different system parameters. Their corresponding parameter regions are represented by I, III, and II, respectively, in Fig. 1(a).[10,11,29,30] In addition, the existence and uniqueness of the limit cycle have been well addressed in standard textbooks of nonlinear dynamics and chaos.[29] The fixed point is locally stable within regions I and II and below the horizontal critical line at $P_m = 1.0$ and, in contrast, the limit cycle is locally stable within regions II and III and above the crooked critical curve. Basically, the horizontal line at $P_m = 1.0$ is recognized as a saddle-node bifurcation, as a pair of a saddle and a node collides and both annihilate after P_m is larger than 1.0. In Refs. 29 and 30, under the condition of larger D, it is further subclassified as an infinite-period bifurcation as the collision of the saddle and node happens exactly at one single loop under the over-damped limit. For the curved critical parameters, it is generally recognized to be a homoclinic bifurcation (or called saddle-loop bifurcation), as the limit cycle collides with the unstable manifold of the saddle and annihilates after that.[35–37]

Although the qualitative picture of the swing equation is clear, quantitative results are still not fully available, including the estimates of the homoclinic bifurcation curve and the approximate analytical solution of the limit cycle. For the first problem, based on the Melnikov method, Guckenheimer and Holmes obtained that it is close to a straight line, $P_m = 4D/\pi$, when D is close to zero, as illustrated by a dashed straight line in Fig. 1(a).[38] However, the deviation from the straight line becomes larger for larger D. In

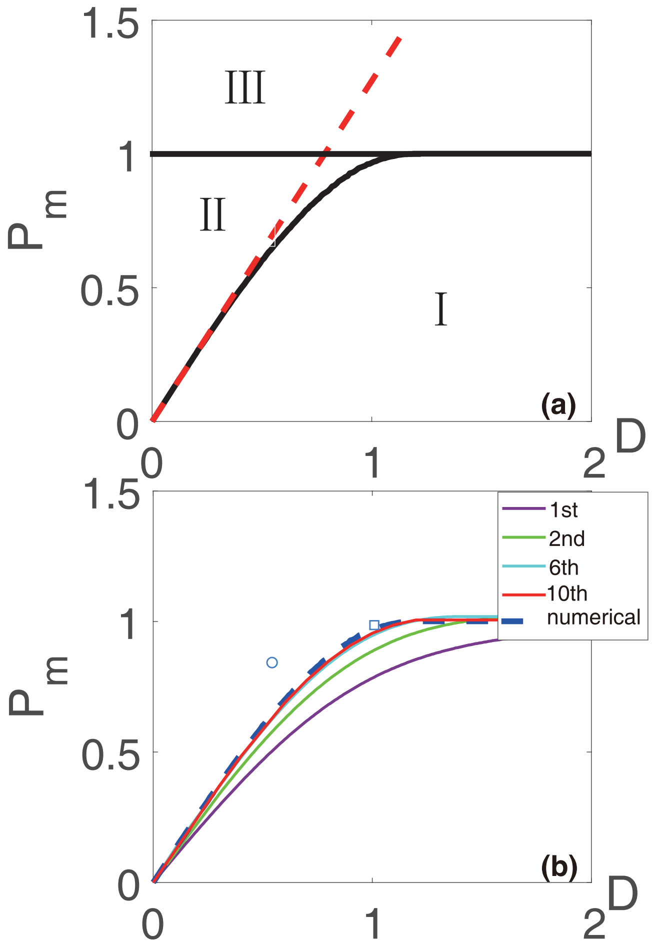

FIG. 1. Phase diagram of the classical second-order swing equation in the $P_m - D$ parameter space, including three different types of dynamical behavior in the three regions: I (for a stable fixed point), II (for coexistence), and III (for a stable limit cycle). The horizontal line at $P_m = 1$ corresponds to the saddle-node bifurcation, and the bent curve starting from the origin corresponds to the homoclinic bifurcation. In (a), a straight dashed line, $P_m = 4D/\pi$, is from the estimate of Guckenheimer and Holmes. In (b), different orders of the IHB form are studied, compared with the numerical result. Additively, two different parameter sets used in the paper: ($D = 0.5$, $P_m = 0.8$) (open circle) and ($D = 1$, $P_m = 0.98$) (open square) are superimposed.

addition, some earlier known estimates are as follows: Tricomi gave upper and lower estimates already in 1933, and Boem provided another estimate.[39] All these results are not very satisfactory. In a recent paper, Skubov *et al.* gave a substantial contribution by using a polynomial approximation, which, however, highly relies on the mathematical derivation.[40]

For the second unsolved problem, as the parameters approach the homoclinic bifurcation curve, the solution of the limit cycle would become much more distorted, making its prediction very difficult. Some studies focused on this problem. For instance, Anup obtained an approximate solution by using the perturbation theory but still treated the swing equation as a weakly nonlinear system.[41] Salas used the elliptic Jacobian function and obtained an analytic solution of a gravity pendulum with damping.[42] In addition, a recent work based on calculating matrix continued fractions was conducted.[31–33]

Because the swing equation belongs to strongly nonlinear systems, the classical techniques, such as the Lindstedt-Poincaré method,[43] the Krylov-Bogoli-Mitropolsky method,[44] and the multi-scale method[45] suiting for weakly nonlinear systems may not solve the problem. The method of the harmonic balance method maintaining only the first harmonic term has also been applied, but it has been found that the estimated result is not satisfactory.[40] If the order of harmonics increases, the mathematical derivation would become very cumbersome and difficult. To solve this puzzle, Lau and Cheung proposed a new method, called the incremental harmonic balance method (IHB), which is a semianalytical and seminumerical algorithm by combining the incremental method and the harmonic balance method.[46] Similar to the classical harmonic balance method, the IHB assumes that the solution of the equation is in the form of harmonics, but it yields the harmonic coefficients by using an iterative calculation of the incremental method, similar to the Newton-Raphson method for solving general nonlinear algebraic equations. By using such a numerical technique, the problem of finding coefficients of different balanced harmonic terms can be efficiently solved by numerical calculation. So far, it has been widely used to solve a variety of strongly nonlinear problems including the van der Pol oscillator, the Duffing oscillator, the beam or plate vibration of large amplitude in various engineering problems, and even the strongly nonlinear fractional-order Mathieu-Duffing equation.[46–52] However, there is no incremental harmonic balance analysis on the swing equation to the best of the authors' knowledge.

In this paper, the IHB method is used to obtain the approximate solution of the limit cycle in the swing equation. Further, the homoclinic bifurcation curve is estimated based on these solutions. Finally, this procedure is extended to study a third-order model of the synchronous generator considering voltage dynamics to verify the validity of the IHB method. The final section is devoted to conclusion and discussion.

II. THE CLASSICAL SWING EQUATION

A. Modeling

According to Newton's second equation of motion, the swing equation for the rotor's motion of a synchronous generator is represented by

$$M\frac{d^2\delta}{dt^2} = -D\frac{d\delta}{dt} + P_m - K\sin\delta, \tag{1}$$

where δ is the rotor angle of the synchronous generator, P_m is the mechanical input active power, M and D denote the inertia and damping of the synchronous generator, respectively, and K represents the coefficient of the electromagnetic energy output to the grid. All parameters are normalized.[7–9]

There are four tunable parameters in Eq. (1). Basically, we can keep any two by using a rescaling. Without losing generality, we choose the mechanical input power P_m and the damping coefficient D as our primary parameters by fixing the other parameters $M = 1.0$ and $K = 1.0$, which are also typical in per-unit in power systems.[28] Then, we obtain

$$\frac{d^2\delta}{dt^2} + D\frac{d\delta}{dt} + \sin\delta = P_m, \tag{2}$$

which is familiar in nonlinear dynamics.[29]

B. Application of the IHB method

Defining $\frac{d\delta}{dt} = \omega = \omega(\delta)$, we have $\frac{d^2\delta}{dt^2} = \frac{d\omega}{dt} = \frac{d\omega}{d\delta}\frac{d\delta}{dt} = \dot{\omega}\omega$, where $\dot{\omega} = \frac{d\omega}{d\delta}$ and it is different from $\frac{d\omega}{dt}$. Thus, we can pass in Eq. (2) to a new independent variable δ,

$$\dot{\omega}\omega + D\omega + \sin\delta = P_m. \tag{3}$$

Next, we intend to determine the periodic solution of $\omega(\delta)$ as a function of δ by using the IHB method.[46–52] As the first step to deal with the incremental, let ω be the solution of Eq. (3) and then its perturbed form as $\omega = \omega + \Delta\omega$. After substituting it into Eq. (3) and omitting all higher order small quantities, we obtain the incremental equation (with $\Delta\omega$ being an unknown quantity),

$$\Delta\dot{\omega}\omega + (\dot{\omega} + D)\Delta\omega = P_m - D\omega - \sin\delta - \dot{\omega}\omega, \tag{4}$$

where $R = P_m - D\omega - \sin\delta - \dot{\omega}\omega$ is called the unbalanced force. Clearly, when ω is the exact solution of the swing equation, $\Delta\omega = 0$ and $R = 0$.

The second step of the IHB method is the harmonic balance process, the same as what we have done in the classical harmonic balance method. It assumes that

$$\omega = a_1 + a_2\cos\delta + a_3\sin\delta + a_4\cos 2\delta + a_5\sin 2\delta + \cdots + a_{2n}\cos n\delta + a_{2n+1}\sin n\delta \tag{5}$$

and

$$\Delta\omega = \Delta a_1 + \Delta a_2\cos\delta + \Delta a_3\sin\delta + \Delta a_4\cos 2\delta + \Delta a_5\sin 2\delta + \cdots + \Delta a_{2n}\cos n\delta + \Delta a_{2n+1}\sin n\delta, \tag{6}$$

where a_i denotes the coefficient of the harmonic terms and n is the highest order of harmonics considered in the calculation. We denote $A = \begin{bmatrix} a_1 & a_2 & \cdots & a_{2n+1}\end{bmatrix}^T$ and $\Delta A = \begin{bmatrix}\Delta a_1 & \Delta a_2 & \cdots & \Delta a_{2n+1}\end{bmatrix}^T$ for the harmonic coefficients of ω and $\Delta\omega$, respectively, and hence

$$\omega = \begin{bmatrix}1 & \cos\delta & \sin\delta & \cdots & \cos n\delta & \sin n\delta\end{bmatrix}A \tag{7}$$

and

$$\Delta\omega = \begin{bmatrix}1 & \cos\delta & \sin\delta & \cdots & \cos n\delta & \sin n\delta\end{bmatrix}\Delta A. \tag{8}$$

We should also express R in Eq. (4) into the harmonic form and get the corresponding harmonic coefficients, namely,

$$R = \begin{bmatrix}1 & \cos\delta & \sin\delta & \cdots & \cos n\delta & \sin n\delta\end{bmatrix}R_m, \tag{9}$$

where R_m is a column vector. Note that R_m depends on A (not ΔA).

The objective of the next manipulation is to determine ΔA on the basis of the already known A and under the restriction of harmonic balance conditions. Substituting Eqs. (7)–(9) into Eq. (4) and

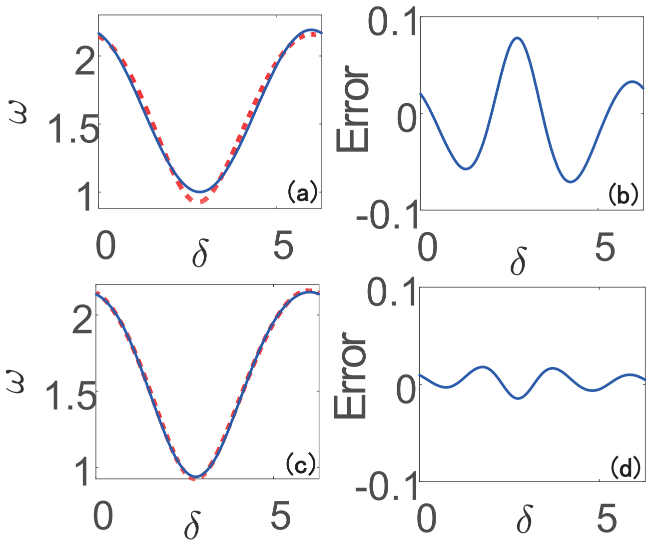

FIG. 2. (a) Comparison of estimated solution (solid curve) and numerical result (dotted curve) for the first-order IHB method and (b) the corresponding error. (c) and (d) The same as (a) and (b), but for the second order IHB method instead. Comparatively, the error has been greatly reduced with the increase of order. The parameters are $D = 0.5$ and $P_m = 0.8$ [an open circle in Fig. 1(b)], typical within the region of the stable limit cycle.

ignoring all higher harmonics, we obtain

$$Z_m \Delta A = R_m, \tag{10}$$

where Z_m is the coefficient matrix of the corresponding harmonic term.

In the calculation, an arbitrarily chosen set of coefficients (A) is given as the initial value of iteration, and ΔA can be solved in the linear algebraic equations [Eq. (10)] with known Z_m and R_m. Namely, a low order solution of ω as a function of δ is first obtained. Then, replacing A with $A + \zeta \Delta A$, with ζ being the iteration coefficient, and substituting it into Eq. (10) to obtain the new ΔA. In this iterative procedure, as Z_m and R_m in Eq. (10) depend on A, they should be updated in each iterate. Repeat these steps until the norm of the imbalanced force R_m approaches zero. Note that here the choice of ζ $(0 < \zeta < 1)$ depends on the value of D; to avoid the situation that the imbalanced force R does not converge, we should choose a smaller ζ. In general, the smaller ζ is, the more iterations are calculated and higher accuracy is obtained. To clearly show the whole calculation process, a detailed flow chart of the IHB algorithm is exhibited in the Appendix. In addition, we have uploaded all relevant program codes and data in Figshare.[53]

C. Approximate analytic solutions of the limit cycle

Before analyzing the bifurcation of the limit cycle, we first illustrate the procedure by computing the limit cycles for a fixed set of parameters $D = 0.5$ and $P_m = 0.8$. These parameters are arbitrarily adopted within region II and illustrated by an open circle in Fig. 1(b). Let us consider the simplest first-order IHB model with the first form, $\omega = a_1 + a_2 \cos\delta + a_3 \sin\delta$, and by using the above IHB algorithm, we get

$$\omega = 1.6000 + 0.5638 \cos\delta - 0.1780 \sin\delta. \tag{11}$$

Meanwhile, to make a comparison, we use an explicit Runge-Kutta (4,5) algorithm to obtain the numerical solution of the original system (2). The error is defined as their mismatch,

$$\text{error} = x_i - y_i, \tag{12}$$

where x_i and $y_{i(i=1,\ldots,N)}$ are the two time series calculated by the IHB method and the numerical solution, respectively, and N is the total number of data. The corresponding estimated solution (solid curve) and the numerical result (dotted curve) are illustrated in Fig. 2(a) with their corresponding error results in Fig. 2(b).

In order to further reduce the error, we may choose the second order IHB and obtain

$$\begin{aligned}\omega = 1.600 &+ 0.5768 \cos\delta - 0.1850 \sin\delta - 0.0402 \cos 2\delta \\ &+ 0.0395 \sin 2\delta,\end{aligned} \tag{13}$$

whose results are shown in Figs. 2(c) and 2(d), where we can see that the error is indeed substantially reduced, compared to that of the first-order result of the top two panels.

Next to systematically characterize the error of different orders of the IHB method, we introduce the mean squared error (MSE),[54]

$$\text{MSE} = \frac{1}{N}\sum_{i=1}^{N}(x_i - y_i)^2. \tag{14}$$

Table I summarizes the predicted coefficients of each harmonic term and its corresponding MSE. It obviously shows that with the increase of the harmonic terms, more precise approximation results are obtained. For instance, the value of MSE has sharply dropped from 0.002 32 to 0.000 02, when a third order IHB is included.

So far, by using the IHB method, we have already obtained an almost perfect approximation result for one set of system parameters of $D = 0.5$ and $P_m = 0.8$, which is far away from the homoclinic

TABLE I. Harmonic coefficients and corresponding MSE obtained by different orders of the IHB method (from first to third); $D = 0.5$ and $P_m = 0.8$, typical within the region of the stable limit cycle.

Items	Constant term	cosδ	sinδ	cos 2δ	sin 2δ	cos 3δ	sin 3δ	MSE
1	1.6000	0.5638	−0.1780					0.002 32
2	1.6000	0.5768	−0.1850	−0.0402	0.0395			0.000 09
3	1.6000	0.5771	−0.1855	−0.0412	0.0414	0.0039	−0.0103	0.000 02

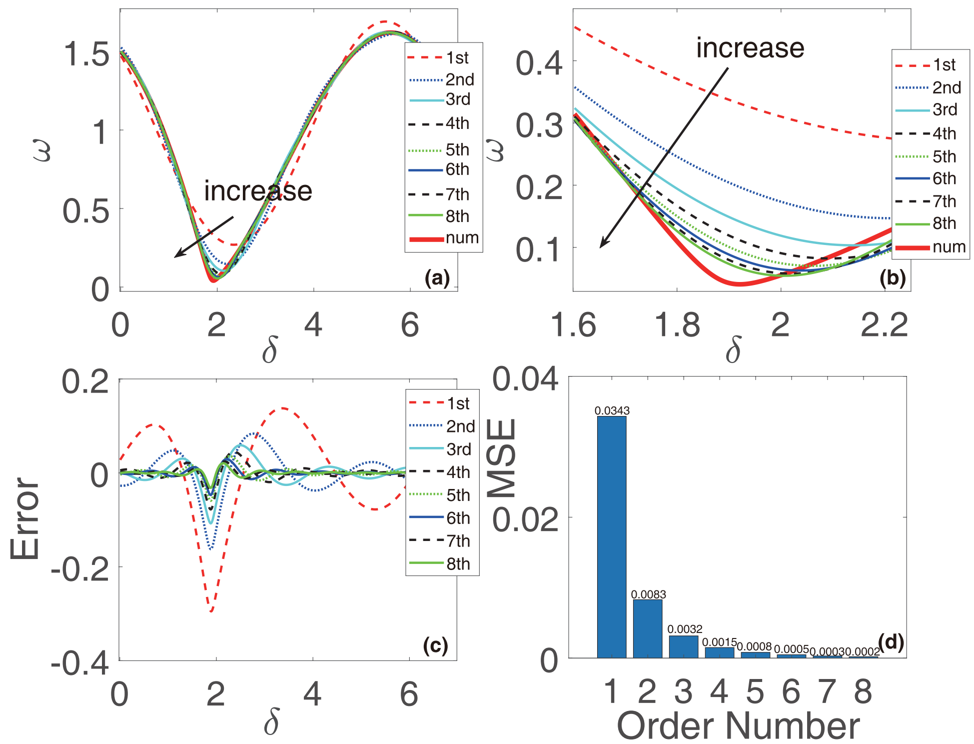

FIG. 3. (a) Comparison and (b) its zoom-in of numerical and approximate results for different orders. The parameters are $D = 1$ and $P_m = 0.98$ [an open square in Fig. 1(b)], which are closer to the homoclinic bifurcation line. (c) and (d) Plots of error and MSE, to show the detail of the approximate effect, respectively. Clearly, a better estimate can be achieved with an increase of the calculation order.

bifurcation line and within the stable regions of the limit cycle. When the parameters are moved closer to the homoclinic bifurcation line, we find that the IHB method is still workable, but a much higher order of harmonics should be included. As one example, the parameters $D = 1$ and $P_m = 0.98$ are chosen, as illustrated by an open square in Fig. 1(b). The comparison of the numerical result (heavy solid curves) and approximate results for different orders is given in Fig. 3(a). Their corresponding magnification and the results of error and MSE are shown in Figs. 3(b)–3(d). It is clear that now the periodic motion becomes much more seriously distorted, quite different from the sinusoidallike wave form in Fig. 2. Thus, to obtain a higher degree of accuracy, we need to increase the order of harmonics. All different order results given in Fig. 3 clearly show that they approach the numerical result gradually, with a sharp decrease of the value of MSE. In addition, to be specific, we list all obtained coefficients of each harmonic term and their corresponding MSE in Table II.

D. Prediction of the homoclinic bifurcation curve

We have seen that the IHB method is efficient to solve the problem of the approximate analytic solution of the limit cycle for any system parameters, either close to or far away from the homoclinic bifurcation curve within the stable region. Next, we like to use these approximate solutions to directly solve the problem of prediction of the homoclinic bifurcation curve.

TABLE II. Harmonic coefficients and corresponding MSE obtained by different orders of the IHB method (from first to eighth); $D = 1$ and $P_m = 0.98$, being quite close to the homoclinic bifurcation line.

Items	Constant term	$\cos\delta$	$\sin\delta$	$\cos 2\delta$	$\sin 2\delta$	$\cos 3\delta$	$\sin 3\delta$	$\cos 4\delta$	$\sin 4\delta$	$\cos 5\delta$	$\sin 5\delta$	$\cos 6\delta$	$\sin 6\delta$	MSE
1	0.9800	0.4949	−0.5101											0.0343
2	0.9800	0.4843	−0.5265	0.0643	0.0993									0.0083
3	0.9800	0.4797	−0.5386	0.0798	0.0994	−0.0427	0.0121							0.0032
4	0.9800	0.4784	−0.5387	0.0833	0.0974	−0.0465	0.0201	0.0086	−0.0220					0.0015
5	0.9800	0.4780	−0.5386	0.0841	0.0963	−0.0464	0.0230	−0.0028	−0.0261	0.0019	0.0045			0.0008
6	0.9800	0.4778	−0.5385	0.0844	0.0958	−0.0460	0.0240	−0.0047	−0.0269	0.0153	0.0033	−0.0051	0.0062	0.0005
7	0.9800	0.4777	−0.5385	0.0844	0.0956	−0.0457	0.0244	−0.0056	−0.0270	0.0164	0.0022	−0.0051	0.0087	0.0003
8	0.9800	0.0477	−0.5385	0.0844	0.0955	−0.0455	0.0246	−0.0060	−0.0270	0.0167	0.0016	−0.0047	0.0098	0.0002

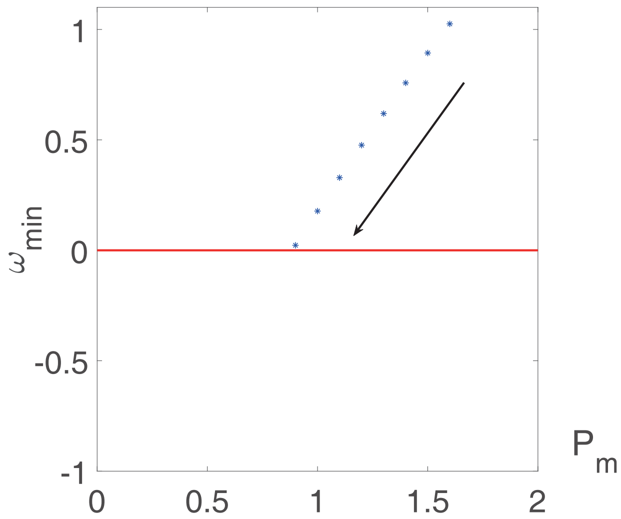

FIG. 4. Plot of ω_{min} vs P_m with P_m decreasing from 1.6 to 0.9 and $\Delta P_m = -0.1$; the value of ω_{min} is the minimum of the estimated ω vs δ for the corresponding P_m. $D = 1.0$ is fixed. Based on this tendency, we can infer a critical parameter $P_{m,c} \approx 0.89$ under the current condition of $D = 1.0$.

As we know, the homoclinic bifurcation occurs when the limit cycle collides with the unstable manifold of the saddle located at $[\delta = \arcsin(P_m), \omega = 0]$, and it annihilates after the collision. The minimal value of $\omega(\delta)$, ω_{min}, gradually decreases when the system parameters approach the homoclinic bifurcation curve; this point is clear, if we compare the results in Figs. 2 and 3. In particular, ω_{min} in Fig. 3 nearly touches the zero value. Therefore, we may choose ω_{min} as an index to characterize the distance from the homoclinic bifurcation, and test whether it is equal to zero as the critical condition for the emergence of the bifurcation.

Figure 4 plots ω_{min} vs P_m with P_m decreasing from 1.6 to 0.9 ($\Delta P_m = -0.1$) and D fixed; $D = 1$. A monotonic decrease of ω_{min} with the decrease of P_m is clear, until a critical predicted value $P_{m,c} \approx 0.89$ arrives. Thus, the homoclinic bifurcation point has been well predicted. Note that, for any $P_m < P_{m,c}$, as the limit cycle is locally unstable, we cannot obtain any significant solution of the limit cycle any longer. With this single-side data for a fixed D as that in Fig. 4, we can further determine the locus of the whole homoclinic bifurcation curve by scanning the parameter D. The final results are shown in Fig. 1(b), where clearly they are coincident with the numerical results of the original system (2) when a sufficiently high order of harmonics is considered.

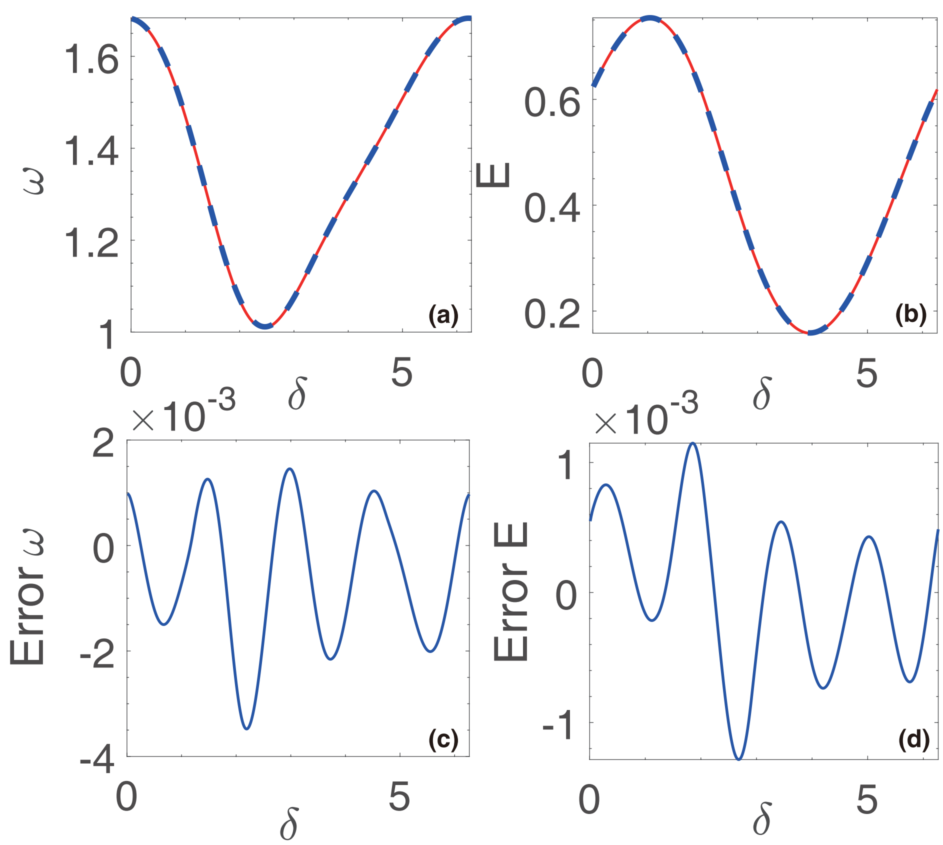

FIG. 5. (a) and (b) Comparison of numerical solution (solid line) and approximate solution (dashed line) of ω and E, respectively, for the generalized swing equation [Eqs. (15)] considering voltage dynamics, with a third-order IHB method. (c) and (d) Errors of ω and E, respectively. The parameters $D = 0.5$ and $P_m = 0.8$ are fixed.

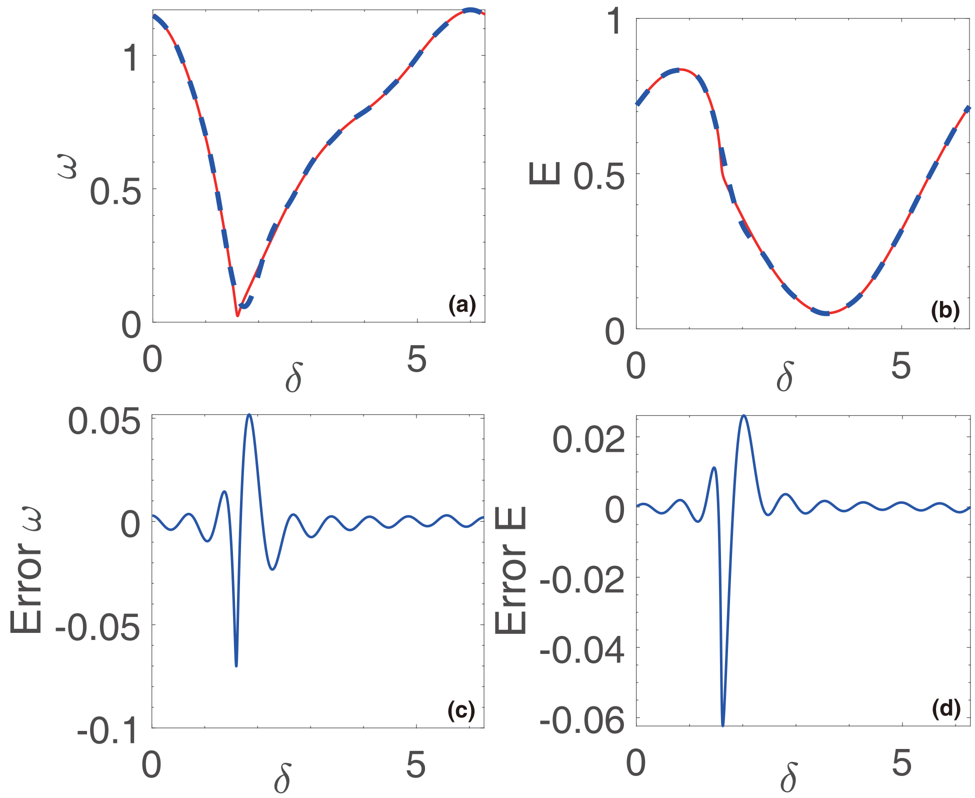

FIG. 6. Similar to Fig. 5, but for a different set of parameters $D = 0.6$ and $P_m = 0.54$ and with a fifth-order IHB method instead. Clearly, when the parameters are closer to the homoclinic bifurcation curve, a more distorted periodic solution of $\omega(\delta)$ is observed, and a higher order of harmonics in the IHB method is needed accordingly.

III. GENERALIZED SWING EQUATION

In this section, we will study a generalized swing equation, namely, a third order model of the synchronous generator incorporating voltage dynamics,[7–11]

$$\begin{aligned} \dot{\delta} &= \omega, \\ M\dot{\omega} &= -D\omega + P_m - BV_s E \sin\delta, \\ T_{d0}\dot{E} &= E_f - (1+XB)E + XBV_s\cos\delta, \end{aligned} \tag{15}$$

where E is the quadrature-axis transient voltage of the synchronous generator, T_{d0} represents the direct-axis open-circuit transient time constant of the synchronous generator, E_f denotes the field excitation voltage, V_s is the voltage at the infinitely strong bus, and B and X are derived system parameters. Different from the classical swing equation, this third order model has been regarded as a more realistic model and has been widely used in power system calculations.

Clearly, now we have the three state variables δ, ω, and E, which can be expressed together as a state vector $\begin{bmatrix}\delta & \omega & E\end{bmatrix}^T$. Similarly, we will choose the mechanical input power P_m and the damping coefficient D as our primary parameters, with all other typical per-unit parameters fixed; $M = 1.0$, $B = 1.0$, $V_s = 1.0$, $E_f = 1.0$, $T_{d0} = 2.0$, and $X = 1.0$.[28] By theoretically analyzing the stability of the fixed points, we obtain the critical parameter for the saddle-node bifurcation: $P_m = 0.6495$.

Let us use the IHB method to solve similar problems in Eq. (15). Changing the variable $\dot{\delta} = \omega(\delta)$, we can pass it to a new independent

TABLE III. Harmonic coefficients and corresponding MSE obtained by different orders of the IHB method in the generalized swing equation [Eq. (15)] considering voltage dynamics (from first to third); $D = 0.5$, $P_m = 0.8$ (open circle in Fig. 7).

Items		Constant term	$\cos\delta$	$\sin\delta$	$\cos 2\delta$	$\sin 2\delta$	$\cos 3\delta$	$\sin 3\delta$	MSE($\times 10^{-6}$)
1	ω	1.3614	0.2947	−0.1082					2034
	E	0.4554	0.1752	0.2382					198.5
2	ω	1.3642	0.2959	−0.1137	0.0289	0.0503			45.95
	E	0.4541	0.1824	0.2359	−0.0159	−0.0031			6.899
3	ω	1.3644	0.2959	−0.1143	0.0296	0.0514	−0.0078	−0.0037	2.160
	E	0.4540	0.1828	0.2357	−0.0165	−0.0023	0.0014	−0.0026	0.3578

TABLE IV. Harmonic coefficients and corresponding MSE obtained by different orders of the IHB method in the generalized swing equation [Eqs. (15)] (from first to third); $D = 0.6$, $P_m = 0.54$ (open square in Fig. 7).

Items		Constant term	cosδ	sinδ	cos 2δ	sin 2δ	cos 3δ	sin 3δ	MSE
1	ω	0.7039	0.3388	−0.2888					0.0525
	E	0.4118	0.3343	0.2353					0.0080
2	ω	0.7331	0.2993	−0.3184	0.1520	0.0712			0.0142
	E	0.4065	0.3488	0.2005	−0.0310	0.0387			0.0045
3	ω	0.7413	0.2844	−0.3187	0.1720	0.0589	−0.0373	0.0470	0.0067
	E	0.4059	0.3468	0.1907	−0.0191	−0.0500	−0.0209	−0.0117	0.0023

variable δ,

$$\begin{aligned} \dot{\omega}\omega &= P_m - D\omega - E\sin\delta, \\ 2\dot{E}\omega &= 1 - 2E + \cos\delta, \end{aligned} \tag{16}$$

where $\dot{\omega} = \frac{d\omega}{d\delta}$ and $\dot{E} = \frac{dE}{d\delta}$.

Let ω and E be the solution of the above equations and express the perturbed ω and E as $\omega = \omega + \Delta\omega$ and $E = E + \Delta E$, we yield the increment equations with $\Delta\omega$ and ΔE,

$$\begin{aligned} \Delta\dot{\omega}\omega + \dot{\omega}\Delta\omega + D\Delta\omega + \Delta E\sin\delta &= R_1, \\ 2\dot{E}\omega + 2\Delta\dot{E}\omega + 2\Delta E &= R_2, \end{aligned} \tag{17}$$

where

$$\begin{aligned} R_1 &= P_m - D\omega - \dot{\omega}\omega - E\sin\delta, \\ R_2 &= 1 - 2E - 2\dot{E}\omega + \cos\delta. \end{aligned}$$

When ω and E are the exact solutions, R_1 and R_2 will vanish.

Under the assumptions of different orders of harmonics, we have

$$\begin{aligned} \omega &= a_1 + a_2\cos\delta + a_3\sin\delta + a_4\cos 2\delta + a_5\sin 2\delta \\ &\quad + \cdots + a_{2n}\cos n\delta + a_{2n+1}\sin n\delta, \\ \Delta\omega &= \Delta a_1 + \Delta a_2\cos\delta + \Delta a_3\sin\delta + \Delta a_4\cos 2\delta \\ &\quad + \Delta a_5\sin 2\delta + \cdots + \Delta a_{2n}\cos n\delta + \Delta a_{2n+1}\sin n\delta, \\ E &= b_1 + b_2\cos\delta + b_3\sin\delta + b_4\cos 2\delta + b_5\sin 2\delta \\ &\quad + \cdots + b_{2n}\cos n\delta + b_{2n+1}\sin n\delta, \\ \Delta E &= \Delta b_1 + \Delta b_2\cos\delta + \Delta b_3\sin\delta + \Delta b_4\cos 2\delta \\ &\quad + \Delta b_5\sin 2\delta + \cdots + \Delta b_{2n}\cos n\delta + \Delta b_{2n+1}\sin n\delta, \end{aligned} \tag{18}$$

where n denotes the order of the IHB method. Substituting them into Eqs. (17) and ignoring high harmonics, we can determine the coefficients of the same harmonic terms, based on the harmonic balance

$$Z_m\left[\Delta A \quad \Delta B\right]^T = \left[R_{m1} \quad R_{m2}\right]^T, \tag{19}$$

where

$$\begin{aligned} \Delta A &= \left[\Delta a_1 \quad \Delta a_2 \quad \cdots \quad \Delta a_{2n+1}\right], \\ \Delta B &= \left[\Delta b_1 \quad \Delta b_2 \quad \cdots \quad \Delta b_{2n+1}\right]. \end{aligned}$$

Similarly, R_{m1} and R_{m2} are the corresponding column vectors of R_1 and R_2, respectively. Furthermore, similar to the calculation process of the classical swing equation, all coefficients of the harmonics are obtained by an iterative calculation until the norms of R_1 and R_2 are sufficiently small.

As two examples, the results for the parameters of $D = 0.5$ and $P_m = 0.8$ corresponding to the cases far away from the homoclinic bifurcation curve and those of $D = 0.6$ and $P_m = 0.54$ representing the cases close to the homoclinic bifurcation curve are shown in Figs. 5 and 6, respectively. Both show an almost perfect coincidence of the approximate analysis with the numerical result. Meanwhile, we find that for the former sinusoidallike periodic trajectory, a third-order approximation is sufficient, whereas for the latter distorted one, a fifth-order approximation is needed. To be specific, we list the coefficients of each harmonic term for these different cases in Tables III and IV, respectively.

Similar to the classical swing equation, the parameter space of the third-order model can be divided into the fixed point region, the bistable region, and the limit cycle region. The boundary between the fixed point region and the bistable region is the homoclinic

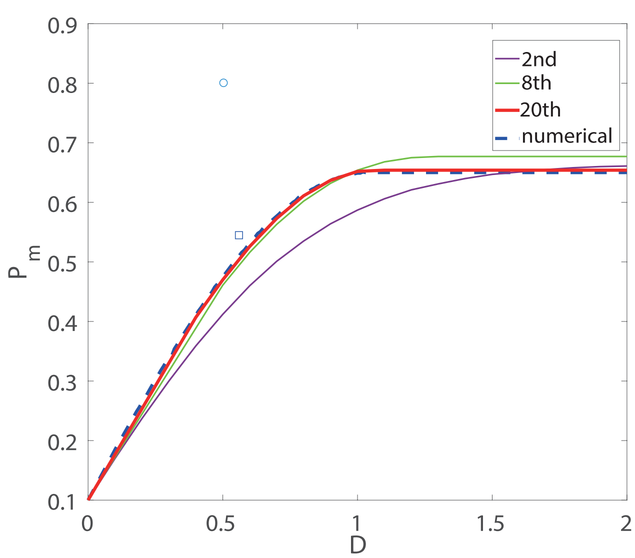

FIG. 7. Comparison of numerical and predicted results for the bifurcation curve of the generalized swing equation. Two parameter sets $D = 0.5$, $P_m = 0.8$ (open circle) and $D = 0.6$, $P_m = 0.54$ (open square) used in the paper are emphasized.

bifurcation line. Finally, let us deal with the estimation of the homoclinic separatrix. Again we select the same criterion as that of the classical swing equation, namely, whether the minimum value of the obtained analytic solution of $\omega_{\min}$ approaches zero. By analyzing $\omega_{\min}$ for different P_m's and D's, we identify the whole homoclinic bifurcation line. The result is shown in Fig. 7, with a clear satisfactory coincidence of the prediction with the numerical result, when a higher order is included.

IV. CONCLUSION AND DISCUSSIONS

In summary, the approximate solution of the limit cycle and the estimate of the homoclinic bifurcation line in the classical swing equation and the generalized swing equation are obtained by using the incremental harmonic balance method. All of these predictions are found to be in good agreement with the numerical results of the full systems in Eqs. (2) and (15). For better precision, a higher order of harmonics in the IHB method could be considered and performed, and this manipulation is efficient with the aid of a computer. Therefore, the two unsolved problems in the classical swing equation have been successfully solved in a unified manner. It is notable that the swing equation belongs to strongly nonlinear systems, which generally cannot be solved by the classical techniques for weakly nonlinear systems.

Here, we admit that the physical picture of the swing equation including a fixed point, a limit cycle, and their coexistence for the variation of system parameters has been well-known before. Even back to the period of Poincaré over 100 years ago, the homoclinic bifurcation, saddle-node bifurcation, and existence and uniqueness of the limit cycle have been well addressed, according to the introduction of Strogatz in his famous textbook of nonlinear and chaotic dynamics.[29] Thus, all analytical (or semianalytical) methods for approximated solutions of periodic motions try to obtain an explicit form. This could provide an improved physical insight and is also very important and helpful for many engineering problems.

Finally, as the power system has become more power-electronics-based and how to deal with the grid dynamics when generators are connected to distributed renewable sources of energy is important,[1,55] we hope that the quantitative results provided in this paper could be helpful for our understanding of complicated dynamics of not only traditional power systems but also power-electronics-based power systems. We also expect that this method could be generalized to study other similar complex networked dynamical systems, which are usually featured with the nature of a high nonlinearity.

ACKNOWLEDGMENTS

The authors thank the two reviewers very much for their comments and suggestions. This work was partially supported by the National Key Research and Development Program of China under Grant No. 2017YFB0902000, and the International (Regional) Cooperation and Exchange Program of the National Natural Science Foundation of China (Research on Inter-Organizational Cooperation: NSFC-DFG) under Grant No. 11861131011.

APPENDIX: FLOW CHART OF THE IHB ALGORITHM

A flow chart illustrating the major steps of IHB is shown in Fig. 8, with the classical swing equation as an example.

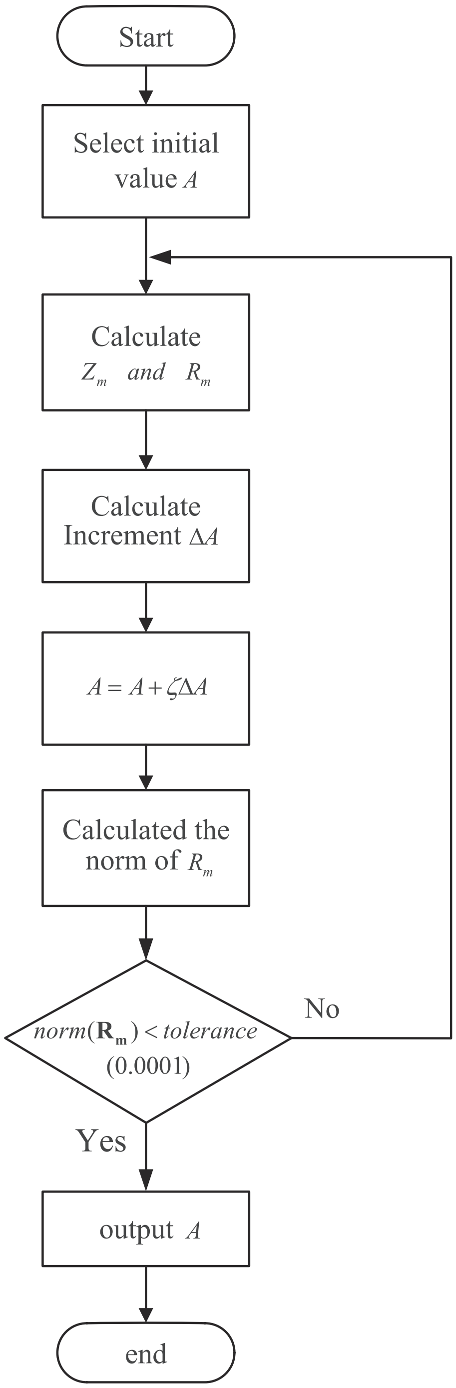

FIG. 8. Flow chart of IHB.

REFERENCES

[1] J. A. Turner, "A realizable renewable energy future," Science **285**, 687–689 (1999).
[2] X. Wang, F. Blaabjerg, and W. Wu, "Modeling and analysis of harmonic stability in an ac power-electronics-based power system," IEEE Trans. Power Electron. **29**, 6421–6432 (2014).
[3] X. Yuan, J. Hu, and S. Cheng, "Multi-time scale dynamics in power electronics-dominated power systems," Front. Mech. Eng. **12**, 303–311 (2017).
[4] M. Zhao, X. Yuan, J. Hu, and Y. Yan, "Voltage dynamics of current control time-scale in a VSC-connected weak grid," IEEE Trans. Power Syst. **31**, 2925–2937 (2015).
[5] W. He, X. Yuan, and J. Hu, "Inertia provision and estimation of PLL-based DFIG wind turbines," IEEE Trans. Power Syst. **32**, 510–521 (2016).
[6] F. Blaabjerg, R. Teodorescu, M. Liserre, and A. V. Timbus, "Overview of control and grid synchronization for distributed power generation systems," IEEE Trans. Ind. Electron. **53**, 1398–1409 (2006).
[7] P. Kundur, N. J. Balu, and M. G. Lauby, *Power System Stability and Control* (McGraw-Hill, New York, 1994), Vol. 7.
[8] L. L. Grigsby, *Power System Stability and Control* (CRC Press, 2016).
[9] J. Machowski, J. Bialek, and J. Bumby, *Power System Dynamics: Stability and Control* (John Wiley & Sons, 2011).
[10] J. Ma, Y. Sun, X. Yuan, J. Kurths, and M. Zhan, "Dynamics and collapse in a power system model with voltage variation: The damping effect," PLoS ONE **11**, e0165943 (2016).
[11] M. He, W. He, J. Hu, X. Yuan, and M. Zhan, "Nonlinear analysis of a simple amplitude–phase motion equation for power-electronics-based power system," Nonlinear. Dyn. **95**(3), 1–12 (2018).
[12] Q.-C. Zhong and G. Weiss, "Synchronverters: Inverters that mimic synchronous generators," IEEE Trans. Ind. Electron. **58**, 1259–1267 (2010).
[13] J. Alipoor, Y. Miura, and T. Ise, "Power system stabilization using virtual synchronous generator with alternating moment of inertia," IEEE J. Emerg. Sel. Top. Power Electron. **3**, 451–458 (2014).
[14] L. Zhang, L. Harnefors, and H.-P. Nee, "Power-synchronization control of grid-connected voltage-source converters," IEEE Trans. Power Syst. **25**, 809–820 (2009).
[15] S. Y. Caliskan and P. Tabuada, "Uses and abuses of the swing equation model," in *2015 54th IEEE Conference on Decision and Control (CDC)* (IEEE, 2015), pp. 6662–6667.
[16] A. Arapostathis, S. Sastry, and P. Varaiya, "Global analysis of swing dynamics," IEEE Trans. Circuits Syst. **29**, 673–679 (1982).
[17] Y. Susuki, I. Mezić, and T. Hikihara, "Coherent swing instability of power grids," J. Nonlinear Sci. **21**, 403–439 (2011).
[18] H.-D. Chiang, *Direct Methods for Stability Analysis of Electric Power Systems: Theoretical Foundation, BCU Methodologies, and Applications* (John Wiley & Sons, 2011).
[19] A. van der Schaft and T. Stegink, "Perspectives in modeling for control of power networks," Annu. Rev. Control **41**, 119–132 (2016).
[20] P. Monshizadeh, C. De Persis, N. Monshizadeh, and A. J. van der Schaft, "Nonlinear analysis of an improved swing equation," in *2016 IEEE 55th Conference on Decision and Control (CDC)* (IEEE, 2016), pp. 4116–4121.
[21] D. S. Gupta, N. Narahari, I. Boyd, and B. Hogg, "An adaptive power-system stabiliser which cancels the negative damping torque of a synchronous generator," in *IEE Proceedings C (Generation, Transmission and Distribution)* (IET, 1985), Vol. 132, pp. 109–117.
[22] P. Ji, T. K. D. Peron, P. J. Menck, F. A. Rodrigues, and J. Kurths, "Cluster explosive synchronization in complex networks," Phys. Rev. Lett. **110**, 218701 (2013).
[23] A. E. Motter, S. A. Myers, M. Anghel, and T. Nishikawa, "Spontaneous synchrony in power-grid networks," Nat. Phys. **9**, 191 (2013).
[24] Y. Yang, T. Nishikawa, and A. E. Motter, "Small vulnerable sets determine large network cascades in power grids," Science **358**, eaan3184 (2017).
[25] D. Witthaut, M. Rohden, X. Zhang, S. Hallerberg, and M. Timme, "Critical links and nonlocal rerouting in complex supply networks," Phys. Rev. Lett. **116**, 138701 (2016).
[26] K. Sharafutdinov, L. Rydin Gorjão, M. Matthiae, T. Faulwasser, and D. Witthaut, "Rotor-angle versus voltage instability in the third-order model for synchronous generators," Chaos **28**, 033117 (2018).
[27] R. Carareto, M. S. Baptista, and C. Grebogi, "Natural synchronization in power-grids with anti-correlated units," Commun. Nonlinear Sci. Numer. Simul. **18**, 1035–1046 (2013).
[28] K. Schmietendorf, J. Peinke, R. Friedrich, and O. Kamps, "Self-organized synchronization and voltage stability in networks of synchronous machines," Eur. Phys. J. Spec. Top. **223**, 2577–2592 (2014).
[29] S. H. Strogatz, *Nonlinear Dynamics and Chaos: With Applications to Physics, Biology, Chemistry, and Engineering* (CRC Press, 2018).
[30] J. M. T. Thompson, M. Thompson, and H. B. Stewart, *Nonlinear Dynamics and Chaos* (John Wiley & Sons, 2002).
[31] H. Risken, *Fokker-Planck Equation* (Springer, 1996), pp. 63–95.
[32] W. Coffey and Y. P. Kalmykov, *The Langevin Equation: With Applications to Stochastic Problems in Physics, Chemistry and Electrical Engineering* (World Scientific, 2012), Vol. 27.
[33] M. Zarifakis, W. T. Coffey, Y. P. Kalmykov, and S. V. Titov, "Models for the transient stability of conventional power generating stations connected to low inertia systems," Eur. Phys. J. Plus **132**, 289 (2017).
[34] D. Manik, D. Witthaut, B. Schäfer, M. Matthiae, A. Sorge, M. Rohden, E. Katifori, and M. Timme, "Supply networks: Instabilities without overload," Eur. Phys. J. Spec. Top. **223**, 2527–2547 (2014).
[35] S. Schecter, "Numerical computation of saddle-node homoclinic bifurcation points," SIAM J. Numer. Anal. **30**, 1155–1178 (1993).
[36] S.-N. Chow and J. K. Hale, *Methods of Bifurcation Theory* (Springer, 2012), Vol. 251.
[37] J. D. Crawford, "Introduction to bifurcation theory," Rev. Mod. Phys. **63**, 991 (1991).
[38] J. Guckenheimer and P. Holmes, *Nonlinear Oscillations, Dynamical Systems, and Bifurcations of Vector Fields* (Springer-Verlag, NY, 1997).
[39] F. Tricomi, "Integrazione di un'equazione differenziale presentatasi in elettrotecnica," Ann. Scuola Norm. Sci. **2**, 1–20 (1933).
[40] D. Skubov, A. Lukin, and I. Popov, "Bifurcation curves for synchronous electrical machine," Nonlinear Dyn. **83**, 2323–2329 (2016).
[41] S. Anup, T. Bhatti, and A. Verma, "Application of analytical methods to approximate the solution to non-linear rotor angle oscillations of single machine infinite bus system," in *2016 IEEE 1st International Conference on Power Electronics, Intelligent Control and Energy Systems (ICPEICES)* (IEEE, 2016), pp. 1–6.
[42] A. H. Salas *et al.*, "Exact solution to duffing equation and the pendulum equation," Appl. Math. Sci. **8**, 8781–8789 (2013).
[43] H.-M. Liu, "Approximate period of nonlinear oscillators with discontinuities by modified Lindstedt–Poincaré method," Chaos, Solitons Fractals **23**, 577–579 (2005).
[44] T. Kakutani and N. Sugimoto, "Krylov-Bogoliubov-Mitropolsky method for nonlinear wave modulation," Phys. Fluids **17**, 1617–1625 (1974).
[45] A. H. Nayfeh, "Order reduction of retarded nonlinear systems–the method of multiple scales versus center-manifold reduction," Nonlinear Dyn. **51**, 483–500 (2008).
[46] S. Lau and Y. Cheung, "Amplitude incremental variational principle for nonlinear vibration of elastic systems," J. Appl. Mech. **48**, 959–964 (1981).
[47] S. Lau and S. Yuen, "The Hopf bifurcation and limit cycle by the incremental harmonic balance method," Comput. Methods Appl. Mech. Eng. **91**, 1109–1121 (1991).
[48] S. Lau, Y. Cheung, and S.-Y. Wu, "Incremental harmonic balance method with multiple time scales for aperiodic vibration of nonlinear systems," J. Appl. Mech. **50**, 871–876 (1983).
[49] Y. Chen, J. Liu, and G. Meng, "Incremental harmonic balance method for nonlinear flutter of an airfoil with uncertain-but-bounded parameters," Appl. Math. Model. **36**, 657–667 (2012).
[50] Y. Shen, S. Yang, and X. Liu, "Nonlinear dynamics of a spur gear pair with time-varying stiffness and backlash based on incremental harmonic balance method," Int. J. Mech. Sci. **48**, 1256–1263 (2006).
[51] L. Fang, J. Wang, and X. Tan, "Frequency response analysis for closed-loop systems with hysteresis using incremental harmonic balance," in *2016 American Control Conference (ACC)* (IEEE, 2016), pp. 1305–1310.

[52] S.-F. Wen, Y.-J. Shen, X.-N. Wang, S.-P. Yang, and H.-J. Xing, "Dynamical analysis of strongly nonlinear fractional-order mathieu-duffing equation," Chaos **26**, 084309 (2016).
[53] https://figshare.com/articles/The programs of IHB algorithm/10032896.
[54] C. Theobald, "Generalizations of mean square error applied to ridge regression," J. R. Stat. Soc. Ser. B **36**, 103–106 (1974).
[55] C. Wang, C. Grebogi, and M. S. Baptista, "Control and prediction for blackouts caused by frequency collapse in smart grids," Chaos **26**, 093119 (2016).